Experimental and mechanistic investigation of benzene formation during atmospheric pressure flow reactor oxidation of n-hexane, n-nonane, and n-dodecane below 1200 K

Trupti Kathrotia*, Patrick Oßwald, Markus Köhler, Nadezhda Slavinskaya, Uwe Riedel

Combustion and Flame 194, (2018) pp. 426–438

The original publication is available at www.elsevier.com

https://doi.org/10.1016/j.combustflame.2018.05.027

Experimental and mechanistic investigation of benzene formation during atmospheric pressure flow reactor oxidation of n-hexane, n-nonane, and n-dodecane below 1200 K

Trupti Kathrotia*, Patrick Oßwald, Markus Köhler, Nadezhda Slavinskaya, Uwe Riedel

Institute of Combustion Technology, German Aerospace Center (DLR), Pfaffenwaldring 38-40, D-70569 Stuttgart, Germany

*Corresponding author: Trupti Kathrotia

German Aerospace Center *(DLR)*

Pfaffenwaldring 38-40

D-70569 Stuttgart

Germany

Email: trupti.kathrotia@dlr.de

Abstract

The reaction kinetics of three n-alkanes: hexane, nonane, and dodecane are investigated both experimentally and numerically through speciation data obtained in a high temperature flow reactor. The measurements are performed in the temperature range of 750 – 1200 K for three different equivalence ratios (Φ = 0.5, 1.0, and 2.0) and major combustion products, intermediates such as olefins, oxygenates, and a soot precursor benzene have been measured.

Formation of benzene is emphasized in this work at intermediate flame temperatures (in this case below 1200 K). Even though this temperature regime has its importance to technical combustors (e.g. at aero engines), the regime is often not studied except a few flow reactor studies. From the three fuels studied, one can see that the benzene formation increases apparently with fuel stoichiometry as well as with increase in carbon number. Unlike at flame conditions, where propargyl recombination plays an important role in benzene formation, at lower flame temperatures (<1200 K) the benzene formation is a result of reactions through small hydrocarbon species occurring from an even (C_2 + C_4) route. The benzene formation reactions present in the reaction model of current work are n-C_4H_5 + C_2H_3 → C_6H_6 + H_2, n-C_4H_5 + C_2H_2 → C_6H_6 + H, i-C_4H_5 + C_2H_4 → C_6H_6 + H + H_2, i-C_4H_5 + C_2H_2 → C_6H_6 + H, and i-C_4H_5 + C_2H → C_6H_6. Analysis of the mechanism at conditions of present work shows that the benzene formation is dominated by the reactions of i-C_4H_5 + C_2H_4 → C_6H_6 + H + H_2 and i-C_4H_5 + C_2H_2 → C_6H_6 + H, their relative importance being dependent on the temperatures at which C_2H_4 and C_2H_2 is formed. The predictions of the speciation data are also compared with prominent literature reaction models (JetSurF 2.0, POLIMI, and RWTH). It appears that absence of either or both of these two reactions in JetSurF 2.0 and RWTH models leads to noticeably lesser contribution to benzene formation giving maximum deviation observed with the measurements. For the DLR and POLIMI models where benzene predictions are close to the experiments, these two reactions are present.

As a consequence a detailed in-house reaction model, which was already extensively validated against global combustion characteristics, has been tested against the measured speciation data. The model succeeds in reproducing all the measured species and is in good agreement with the measurements. This study identifies the major paths during the oxidation of all three fuels studied and provides valuable database and insight into the product spectrum and prediction of soot precursors.

Keywords: reaction kinetics, flow reactor, reaction mechanism, speciation data, soot precursor, benzene

1. Introduction

The future share of renewable energy supply depends on available conversion and storage technologies [1]. Energy from renewable sources e.g. from wind, solar energy is intermittent in nature and therefore the use of surplus power in energy storage is very important for a secure continuous supply. The power-to-fuel process has promising potential, where CO_2 and electricity is converted to liquid fuels [2, 3]. Another carbon source, and in the context of this work, is use of energy from renewable sources (e.g. biomass) through chemical energy conversion technologies for producing high density liquid hydrocarbons [3, 4].

The demand for synthetic liquid hydrocarbon fuels has increased rapidly, as they provide high energy density fuels and benefit from already existing infrastructures. Main applications include alternatives to fossil based fuels in aviation and road transportation or energy storage [5]. They are typically produced by the Fischer-Tropsch (FT) process from reaction of hydrogen with a carbon source obtained from the renewable feedstock or CO_2 capture techniques. The product spectrum of liquid hydrocarbons obtained from this technology is wide and provides a variety of hydrocarbons in different chemical classes. In this context, large alkanes are studied in this work [3].

The three selected alkanes, namely n-hexane, n-nonane, and n-dodecane, are considered as representative of a continuous distribution of n-alkanes as obtainable from FT-processes and is representative, when influences of the obtainable product distribution should be captured. In this study, we aim to understand the difference or similarities in the intermediate pool that arises from the chemical breakdown of the fuel. This is important for an understanding of the pollutant formation e.g. soot formation, which is dependent on the intermediate pool that determines the first benzene ring formation. The presented mechanism thereby allows for flexible representation of various FT product distributions, consisting of n-alkanes.

The aim of this study is to investigate larger hydrocarbons to identify the intermediate species pool, product spectrum, and benzene formation by considering variation in carbon number i.e. chain length and fuel stoichiometry. The objective is to study these effects at temperature from 750 – 1200 K, i.e. at the lower end of temperatures relevant for technical combustors.

We also aim to investigate, whether the benzene formation is influenced by the fuel structure (in this case chain length of alkanes) and whether its formation routes at intermediate temperatures of present study are different compared to flame temperatures. The influence of fuel structure is often studied at flame conditions [6-18], where temperatures are typically above 1400 K. The benzene chemistry at such temperatures is dominated by propargyl recombination chemistry. This has been successfully revealed in a variety of studies [7, 13, 14, 19]. Previous works from different research groups on benzene formation reactions investigated in fuels of different chemical classes (summarized in Table 1s in the supplemental material) concludes that at flame conditions the propargyl recombination is the most important and prominent route to benzene (with only few fuel dependence exceptions) [6-18]. Most technical combustors cover a very broad span of temperature and stoichiometry conditions due the complex interactions of the turbulent fluid dynamics and chemical kinetics. Time-resolved polycyclic aromatic hydrocarbon (PAH), soot (Laser induced incandescence - LII) [20] and temperature measurements [21] for an aero engine typical swirl burner showed the presence of a significant number of instantaneous cases with temperatures below 1000 K in regions of the combustor that are also identified as PAH and soot formation regions. Unfortunately, the measurements have not been performed simultaneously, so no strict coincidence between the individual events can be drawn. Numerical simulations [22] suggest PAH and benzene formation in these flames starting at temperatures below 1200 K for the selected test case. Reaction kinetics investigations on the reactions governing the benzene formation at lower temperature are surprisingly attended by only a few studies [23-

27]. In this study we investigate the speciation data of three n-alkanes: n-hexane, n-nonane, and n-dodecane in a combustion environment. This study focuses on the importance of small species / radicals in the prediction of pollutants for large hydrocarbons at lower flame temperatures.

1.1 Current status on larger hydrocarbons kinetics

There is a considerable amount of literature available on the three hydrocarbons considered in this study. The present status on modeling and experimental studies on n-hexane, n-nonane and n-dodecane is summarized in Table 1. The ignition delay times of the above three hydrocarbons are well investigated and investigations are available for atmospheric to high pressures (20 – 60 atm) in the temperature range of 700 – 1600 K [28-37]. The characteristic burning velocities are studied mostly at atmospheric conditions [38-40] except for n-hexane (2, 5, and 10 atm) [41]. Surprisingly, at flame conditions, no speciation data is available in literature for any of the three hydrocarbons. Species profiles for the three alkanes are measured in Jet Stirred Reactors (JSR) up to 10 atm and 500 – 1200 K [30, 31, 42, 43]. Although the above mentioned studies cover sufficient experimental conditions required for mechanism development, none of them have measured benzene.

Table 1: Overview of available experiments and reaction models in the literature of the investigated three n-alkanes: n-hexane, n-nonane, and n-dodecane.

n-alkane	**Experiments**				**Reaction Mechanisms**
	Ignition delay times	Burning velocities	Speciation data		
	Shock tube	Flame	Flow reactor	Flame	
n-hexane	700-1200K, 6-42 atm, [28] Φ = 0.5 (1.6 atm); Φ = 1.0 (1.86, 3, 4 atm) [29] Φ = 1,2; 627-1365K; 15, 32 bar; 15 bar (RCM) [30]	353 K; 1 atm [38] 353 K; 1,2,5,10 atm [41] 295-380 K; 0.4-1 atm [39]	JSR, low- high T [42] JSR, 530 – 1160 K; 10 atm; Φ = 0.5, 1, 2 [30]	-	JetSurF 2.0 [44] Dagaut [45] Blanquart [46] LLNL [47]
n-nonane	Φ = 0.5, 1, 2; 530 – 1591 K; 1, 10 atm [31] Φ = 0.5, 1, 2; 1, 10 atm [48] Φ = 0.5, 1, 2; 1168 – 1600 K; 2, 10, 20 atm [32]	403 K; 1 atm [38]	JSR, 500 – 1100K; 1, 10 atm [31]	-	JetSurF 2.0 [44] LLNL [47]
n-dodecane	Φ =0.25, 0.5, 1; 9-58 atm; 786- 1396 K [33]	403 K; 1 atm [38] 400, 470 K; 1 atm	JSR, 550 – 1150 K; Φ = 0.5, 1, 2; 10 bar [43]	-	Dagaut [43] JetSurF 2.0 [44]

	Φ = 0.5, 1; 727 – 1422K; 15-34 atm [34] Φ = 1, 1300 – 1600 K; 2 atm [36] Φ = 0.1 – 2; 838 – 1382 K; 1.71 – 8.63 atm [35] Φ = 0.46 – 2.05; 867 – 1739 K; 19 – 74 atm [37]	[40]	SVPFR, 1000 – 1300 K [49]		LLNL [47] POLIMI [50]

SVPFR: Stanford variable pressure flow reactor, JSR: Jet Stirred Reactor, RCM: Rapid Compression Machine

On the theoretical side, reaction models available are: n-hexane by Dagaut [45], Blanquart [46], LLNL [47] and n-nonane by LLNL mechanism [47]. The JetSurF 2.0 mechanism [44] includes all the three alkanes. The reaction model of n-dodecane can be found in LLNL [47], POLIMI [50], and Dagaut [43]. Only few of the above mechanisms also include pathways to benzene formation [44, 50].

1.2 Current status on benzene formation kinetics

The PAH inception starts from the formation of the smallest aromatic compound: benzene. Though PAH formation is just a part of the entire soot formation process, benzene formation is the limiting step [51]. The reactions responsible for benzene formation vary from C_2 to C_6 species chemistry. The chemical structure of fuels has a major influence on the benzene formation, since depending on the fuel the different alkyl radicals formed are the determining factor on the intermediate pool, consequently leading to benzene [12, 16, 23, 52]. The benzene formation is thus dependent on the fuel itself in addition to the temperature region where they are formed. Thus understanding the structural effect of the fuel on benzene formation plays an important role for fuel design strategies and for soot reduction strategies.

Several reaction pathways to benzene formation are extensively studied, both theoretically and experimentally, in the literature. Most of the direct measurements of benzene available in the literature are in flames and are focused on smaller hydrocarbons (C < 4) [7, 9, 10, 13, 18]. A few studies are involved in direct measurement of benzene in flames with fuels larger than

C > 4 [10-12, 17]. Although at flame temperatures (above ~1400 K) benzene formation is dominated by fuel dependent precursors, the propargyl recombination is the dominating path to benzene ring formation for most fuels [6-18]. In flames, lower temperatures prevail close to the burner surface, where benzene formation possesses high measurements uncertainty [53]. Thus understanding of low to intermediate temperature benzene formation is inadequate through flame studies. This is important because propargyl radicals may not be formed at lower flame temperatures and many other small radicals shall play an important role in the benzene formation. Most efficient studies in this case are flow reactor tests, which can measure fuel conversion at temperatures as low as 900 K [23-27].

The theoretical side, though extensively studied, reveals many uncertainties with respect to the benzene formation pathways e.g. [18]. Inaccuracy in the recombination reactions involving small species influences the benzene formation interpretation heavily. Despite tremendous progress in mechanism development, many reaction models are only capable reproducing the benzene formation over a limited temperature range. Even the well accepted propargyl self-recombination path in different literature mechanism varies where benzene is either directly produced from propargyl self-recombination or via intermediate phenyl or fulvene [7, 9, 10, 13, 54-58]. Among the limited reaction mechanisms of larger hydrocarbons available in the literature that incorporate benzene formation chemistry as well are JetSurF 2.0 [44] and POLIMI [50].

The above discussed studies have shown that formation of benzene is complex involving many different reaction routes owing to temperature and fuel structure. This study provides a discussion on both, the dependence on the fuel´s molecular structure and temperature variation.

2. Experimental and numerical approach

Measurements presented in this work were performed at DLR´s high temperature flow reactor. The experimental setup is previously described in high detail [59, 60], so only a brief description is given here. The system consists of a flow reactor, including gas supplies and vaporizer system, which is coupled to a molecular beam mass spectrometry (MBMS) system. Gases are metered using calibrated mass flow controllers (MFC) while the liquid fuels are regulated volumetrically by a syringe pump. The vaporizer used is consisted of a heated tube (25 mm diameter, 12 cm length) filled with mineral wool where the liquid fuels is directly injected from the syringe to the Ar carrier gas stream. Temperature of the vaporizer was set 50°C below the normal pressure boiling point of the fuel. This was found to be sufficient for stable and complete evaporation of the respective fuel. The system was directly coupled to the reactor inlet flange. Reactor inlet conditions for the three n-alkanes investigated are summarized in Table 2. Conditions were chosen to match a specific molar flow rate (10 slm) and dilution (99% Ar), while fuel and oxidizer flows (O_2) were adjusted to match the intended stoichiometry.

The reactor consists of a ceramic (Al_2O_3) pipe of 1497 mm length and 40 mm inner diameter placed in a high temperature oven. The heated section is 1000 mm in length. Cold reactant gases are fed premixed and pre-vaporized into the reactor. The laminar flowing reactant mixture passes through a known temperature profile before detection of the gas composition as function of the oven temperature (T_{Oven}). Continuous measurements are performed at constant inlet mass flow, while a monotonically decreasing temperature ramp (-200 K/h) is applied to the oven. Due to careful characterization of the system´s behavior i.e. thermal inertia and systematic temperature measurement deviations, a distinct centerline gas phase temperature profile can be assigned for each oven temperature (T_{Oven}) passed through while temperature ramping. The procedure is based on measured temperature profiles and validated

for the present temperature ramp and flow conditions, details can be found in [59]. Note that experimental results obtained for temperature ramping have shown to coincide with those obtained from individual isothermal condition if the system´s thermal inertia is considered properly. Averaging time of the MBMS measurements correspond to a 2.5 K temperature interval.

As a consequence of the above experimental approach, each measured species concentration (at distinct T_{Oven}) refers to a full spatial temperature profile of the flow reactor. This has been considered in the simulations by using these profiles as input parameter to the plug flow reactor calculations [59]. The calculations are performed at oven temperatures from 750 to 1200 K with intervals of 1 K and the species mole fraction exiting the reactor i.e. at 147 cm are plotted for each individual temperature thereby providing the spectrum of the mole fractions against the oven temperature similar to the experimental values. Furthermore, the flow reactor calculations require the initial fuel composition, flow rates and pressure as input parameters. The calculations are performed using Chemical WorkBench (CWB) [61]. This approach has been examined to give reliable results, see e.g. [62-64].

For determination of the composition at the reactor exit, gases were withdrawn by a quartz cone at the centerline of the reactor exit at ambient pressures (atmospheric mean pressure is 960 mbar). Sampling was performed at the end of the reaction segment, roughly 30 mm within the reactor tube via a 50 µm orifice at the quartz nozzle tip. All reactions were quenched immediately due to the expansion into a molecular beam (2 differential pumping stages; 10^{-4} and 10^{-6} mbar). The molecular beam was guided to the ion source of an electron impact (EI) time-of-flight (TOF) mass spectrometer (Kaesdorf, mass resolution R = 3000) and species were detected by their exact mass. For the present study, the ionization energy was set to 12.5 eV (actual peak value of the electron energy distribution) in order to minimize dissociative ionization i.e. fragmentation at the ion source. The system's performance

allowed the determination of the elemental composition (C/H/O) of stable species based on the determination of their exact mass. Note that no further determination of isomeric structures beyond the elemental formula is gained experimentally and assignment of individual molecular structures is solely based on the experience from isomer resolving experiments performed in combustion environments e.g. [65-68] and chemically reasonable analogy. In this work radical species have not been evaluated due to poor S/N ratio.

Quantification of the obtained signals follows well established methods described in references [69-71], i.e. by direct binary (species/Ar) calibration measurements or via estimation of the ionization cross section based on the RICS (relative ionization cross section) method [72]. Direct cold gas calibration was performed in this study for CH_4, C_2H_2, C_2H_4, C_2H_6, C_3H_4 (propyne), C_3H_6, C_3H_8, C_4H_4 (vinyl acetylene), C_4H_6 (1,3-butadiene), C_4H_8 (1-butene), C_6H_{12} (1-hexene), C_7H_8 (toluene), C_7H_{14} (1-heptene), C_8H_{16} (1-octene), C_9H_{18} (1-nonene), $C_{10}H_{20}$ (1-decene), and $C_{11}H_{22}$(1-undecene). All other species were calibrated according to RICS [59, 72] based on the respective 1-alkene for aliphatic or toluene for aromatic species. Major species (H_2O, CO_2, CO, H_2, O_2, and the respective fuel) have been determined according to the internal calibration procedure described in [59], which was based on values obtained within the individual measurement either at low (reactants) or high (products) oven temperatures. The absolute experimental uncertainty of the determined mole fractions was estimated to be below 10% for major species, below 20% for direct calibrated intermediates and could be up to a factor of 2-4 for species calibrated by RICS when the ionization cross section is unknown. Note that mixtures of different isomers contributing to a signal can also increase the measurement uncertainty for this elemental composition. Relative comparison between the measurement series exhibited a significantly higher precision i.e. better than 10% uncertainty.

Table 2: Reactor initial conditions, 9900 sccm (standard cubic centimeter per minute at 1013 mbar, 273 K) argon are added as diluent for all measurements.

Φ	**Fuel (gas)** (sccm)	**O_2** (sccm)	**Fuel (liquid)** (µl/min)
		n-C_6H_{14}	
0.5	4.98	95.0	28.9
1.0	9.48	90.5	55.1
2.0	17.3	82.6	100.6
		n-C_9H_{20}	
0.5	3.34	96.5	27.4
1.0	6.63	93.3	52.9
2.0	12.4	87.5	99.2
		n-$C_{12}H_{26}$	
0.5	2.62	97.4	26.5
1.0	5.11	94.9	51.7
2.0	9.72	90.2	98.4

3. Reaction mechanism

The reaction mechanism is a database of elementary reactions which describes the path from vaporized fuel via intermediate species to the final products such as H_2O, CO_2, as well as pollutants. This reaction model is developed in a systematic and hierarchical manner and is validated in an iterative process against the characteristics combustion experiments such as ignition delay times, laminar flame speeds, and speciation data obtained in the flow reactor and flames. The reaction model is first validated against global characteristics and is subsequently modified to increase the validity range of the model (T, p, Φ) and speciation data to provide a strict test.

An in-house reaction mechanism of n-dodecane [73] has been updated in this work to include reactions of n-hexane and n-nonane conversion. The sub-mechanism of both of these species

includes the fuel C_6H_{14}, C_9H_{20} as well as radicals formed such as C_9H_{19}, C_9H_{17}, C_8H_{17}, olefin C_9H_{18}, and the species for low temperature peroxy chemistry. The reactions of both these alkanes are based on the analogy of smaller alkanes and their reactions rates are adapted from the work of Westbrook et al. [74], JetSurF 2.0 mechanism [44], and from Nehse [75]. The DLR in-house benzene and aromatic species reaction mechanism is described in detail elsewhere [15].

The reaction mechanism has been optimized to improve intermediate species prediction as well as the prediction of global combustion characteristics. The following changes are implemented in the present work. More details on changes are also available in supplemental material (Table 2s).

(1) In the initial reaction model of present work [15], C_4H_5 species has been lumped as total of both iso- and n-C_4H_5 isomer. The reaction model was updated to separate both C_4H_5 isomers as it is important for the correct prediction of C_4H_4, C_4H_6 species and, subsequently, to describe benzene formation at the temperatures of the present work. Accordingly, the reaction rates of C_4H_6 H-abstraction rates leading to C_4H_6 + R → n-/i-C_4H_5 + RH have also been updated.

(2) The reaction model is modified to improve predictions of intermediate species. The reactions updated are (1) $CH_2HCO + O_2 = CH_2CO + HO_2$, (2) $C_3H_5 + HO_2 = OH + HCO + C_2H_4$ is replaced by $C_3H_5 + HO_2 = C_3H_6 + O_2$, (3) $C_4H_4 + O = C_3H_4 + CO$ removed, (3) reactions of n-C_4H_5, i-C_4H_5 and C_4H_6 updated, (4) $C_6H_{11} + HO_2 = CH_2O + OH + C_5H_9$ replace by $C_6H_{11} + HO_2 = C_6H_{10} + H_2O_2$, (5) $C_2H_4 + OH = CH_3CHO + H$ removed, and (6) reaction rates of C_4H_5 isomers + $C_2H/C_2H_2 = C_6H_6$ is updated.

(3) The decomposition reaction rate of benzene, phenyl(+H) = $C_2H_2 + C_4H_4$ in the initial mechanism was adapted from [76] recommended for high temperatures (1200 - 2500 K) and was implemented to be a benzene decomposition pathway at high

temperatures. However, the reverse high reaction rate greatly exaggerated the rate of formation of benzene from the two stable molecules (C_2H_2 and C_4H_4) at lower temperatures. Since the contribution of this reaction to benzene formation or consumption is unlikely, this reaction is removed from the initial mechanism.

In the *Results and Discussion* section the model predictions are often compared with available literature reactions mechanisms such as JetSurF 2.0 [44], POLIMI [50], and RWTH [77] mechanisms.

4. Combustion product spectrum – Results and discussion

Comparisons of measured and computed species profiles obtained in the flow reactor are presented in the following. The comparison is shown for species mole fraction as a function of respective oven temperature at a given stoichiometry. To facilitate comparison of the respective trends, a scaling factor (model data scaled roughly to maximum experimental value) is indicated, when applied. Note that no shift in temperature is used.

4.1 Fuel, oxidizer, and major combustion products

The fuel and oxidizer conversion, and major products H_2O, CO_2, and CO formation for the three studied fuels are presented in Fig. 1 and compared to the modeling results. The comparison shows that the fuel and oxidizer conversion and corresponding major product formation at given condition is very well captured by the model.

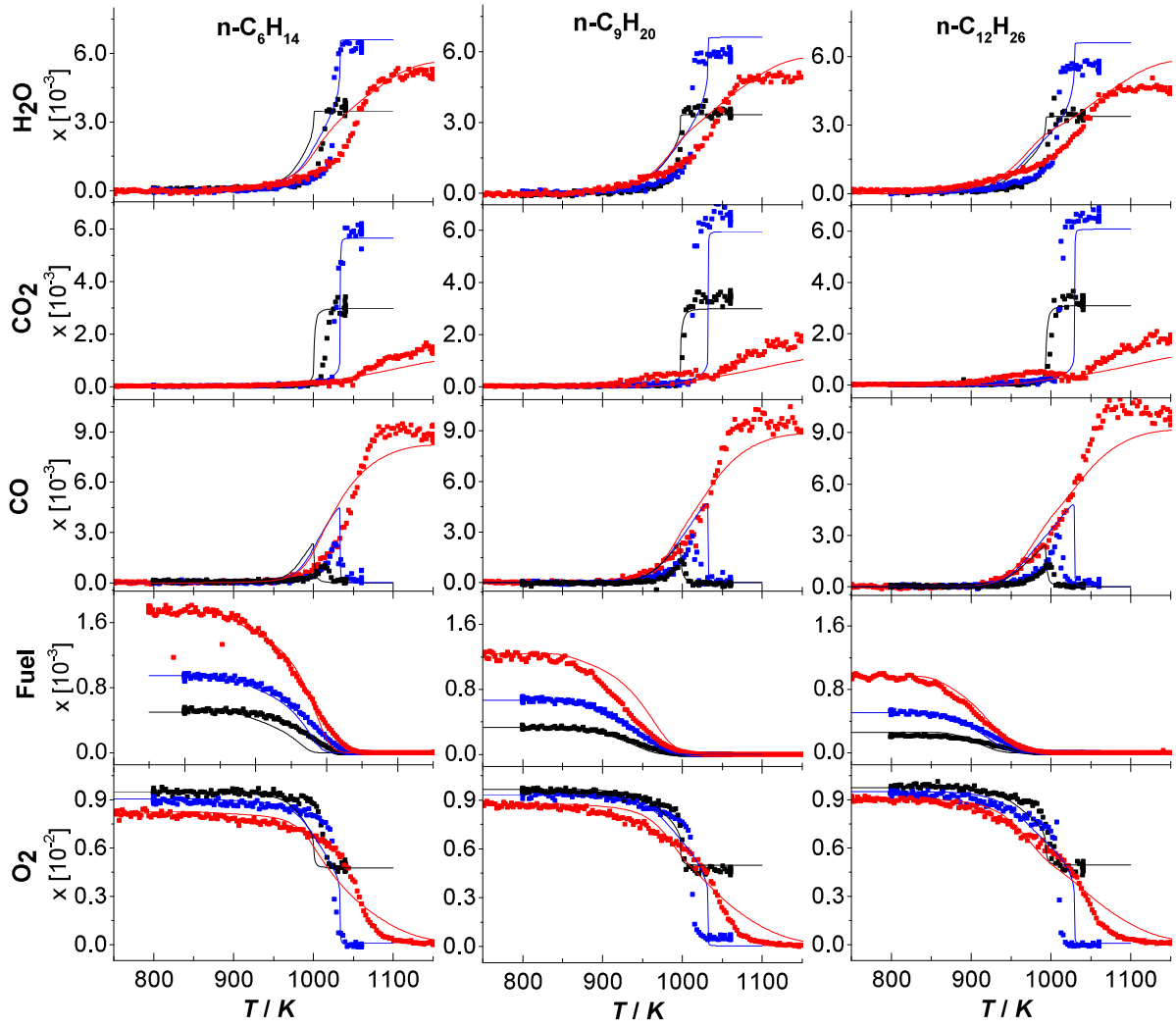

Fig. 1: Mole fraction profiles of fuel, O_2, and major products CO, CO_2, and H_2O as a function of the oven temperatures for the three fuels studied and Φ = 0.5, 1.0, and 2.0. Symbols represent experimental data and lines modeling results. Legend: Φ = 0.5 (black), 1.0 (blue), 2.0 (red).

The intermediate product spectrum depends on the initial fuel molecule and can be understood by the detailed reaction flow analysis. Figure 2 shows at about 50% fuel conversion, that the fuels n-hexane, n-nonane, and n-dodecane are consumed by the H-abstraction reaction to first fuel radicals C_6H_{13}, C_9H_{19}, and $C_{12}H_{25}$, respectively. All these radicals formed are decomposed by ß-scission to one alkyl radical and an olefin. The olefins are also measured in the experiments and are compared with model predictions (s. Figs. 5 and 6). Olefins are important intermediates as they decompose to produce radicals that can form

benzene. The measured olefins are not only validation data for the model, but also provide information on the benzene precursors that are formed from it. Figure 2 shows the species spectrum in the first reaction steps predicted by the model.

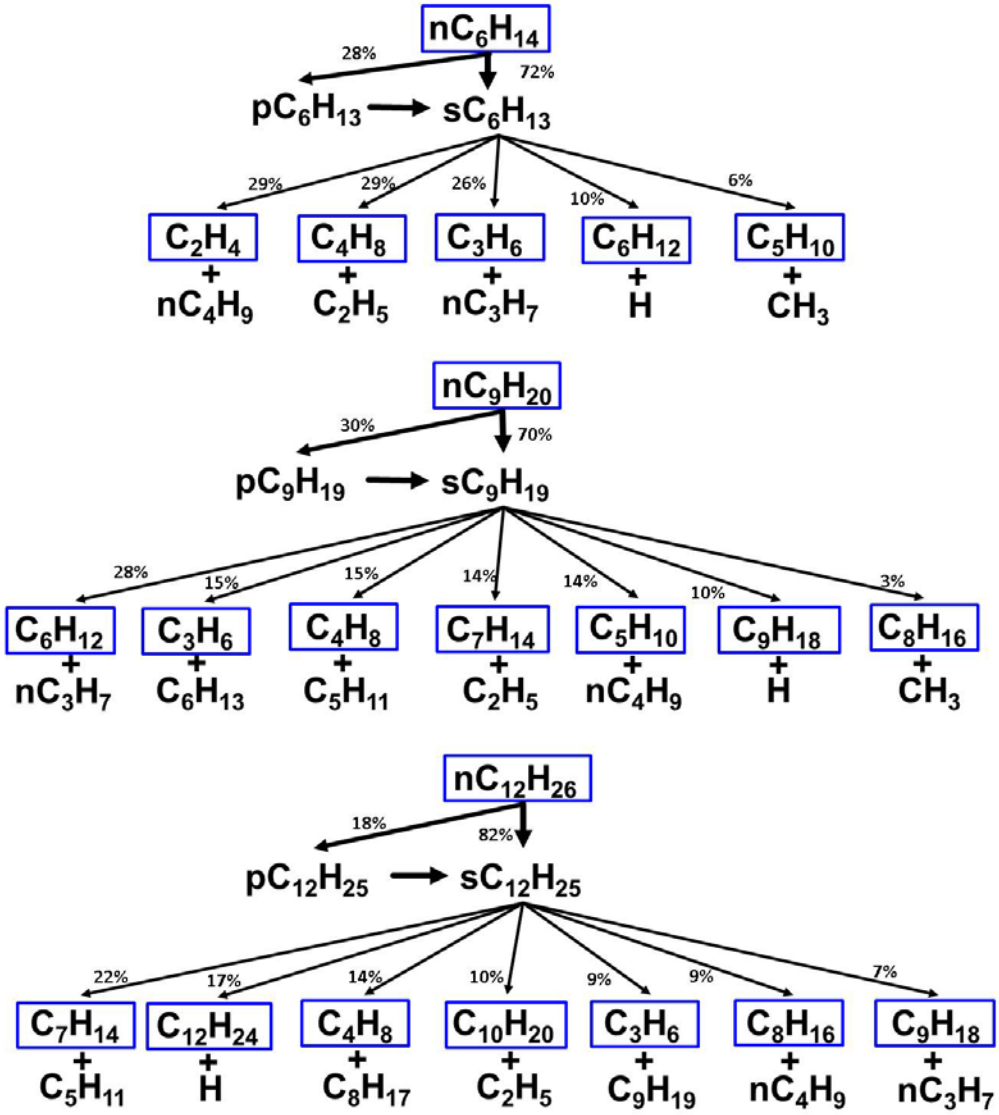

Fig. 2: Reaction path analysis for the three fuels studied when about 50% fuel conversions are achieved in the flow reactor. The fuel decomposition paths are very similar for all three fuel stoichiometries. The species marked with blue boxes are measured in the flow reactor. Species nomenclature: p (primary), s (secondary) carbon site. As an example, pC_9H_{19} and sC_9H_{19} implies lumped primary and secondary C_9H_{19} radicals respectively.

4.2 Intermediate species C_0-C_6

Selected intermediate species are compared by their peak mole fractions in Fig. 3. The measured maximum species mole fractions are shown as columns whereas the corresponding model predictions are shown by symbols. Both the mole fraction and temperature-axis are kept to same values in all 9 cases considered, to allow a direct comparison of influence of change in fuel stoichiometry or fuel carbon number. For all three fuels considered, the influence of fuel stoichiometry is more prominent than the difference in maximum mole fractions due to increase in carbon number. The change in carbon number has nearly no influence for species C ≤ 4. For species with C = 5, 6 the changes are very small and their mole fractions increase with increasing carbon number. All the simulated species are in good agreement with the measured results.

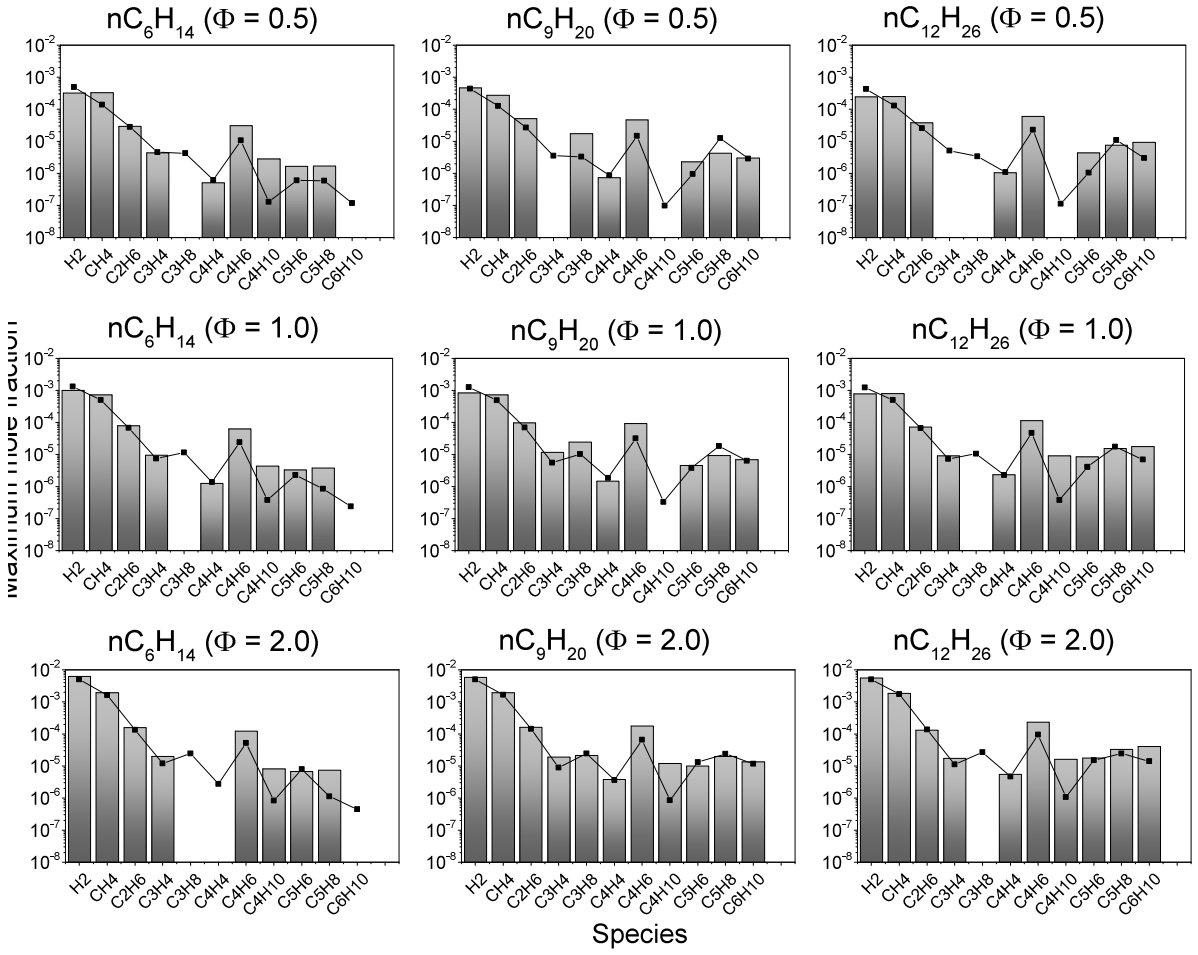

Fig. 3: Maximum measured and predicted mole fraction of intermediate species formed during the conversion of the three fuels studied. Column: experiment, symbol: simulation. The species mole fractions over the entire measured temperatures are available in the supplemental material.

A complete and comprehensive comparison of each species mole fractions profiles is available in the supplemental material.

4.3 Oxygenates

Carbonyl compounds such as formaldehyde (CH_2O), ketene (CH_2CO), and acetaldehyde (CH_3HCO) are oxygenated intermediates formed during the combustion. They are considered hazardous and can be emitted as a result of incomplete combustion in engines. The mentioned three carbonyl compounds are measured for all three stoichiometries. A comparison of measured and simulated carbonyl compounds are presented in Fig. 4. For all the three compounds, their formation increases with fuel stoichiometry and a slight increase is seen with increase in the carbon number of the fuel. The simulated formaldehyde mole fractions are a factor of 2 higher compared to the measurements, whereas the ketene and acetaldehyde are roughly twice under-predicted by model. Note that the increased error tolerance coming with the RICS calibration of those species brings the model results close to the error limits.

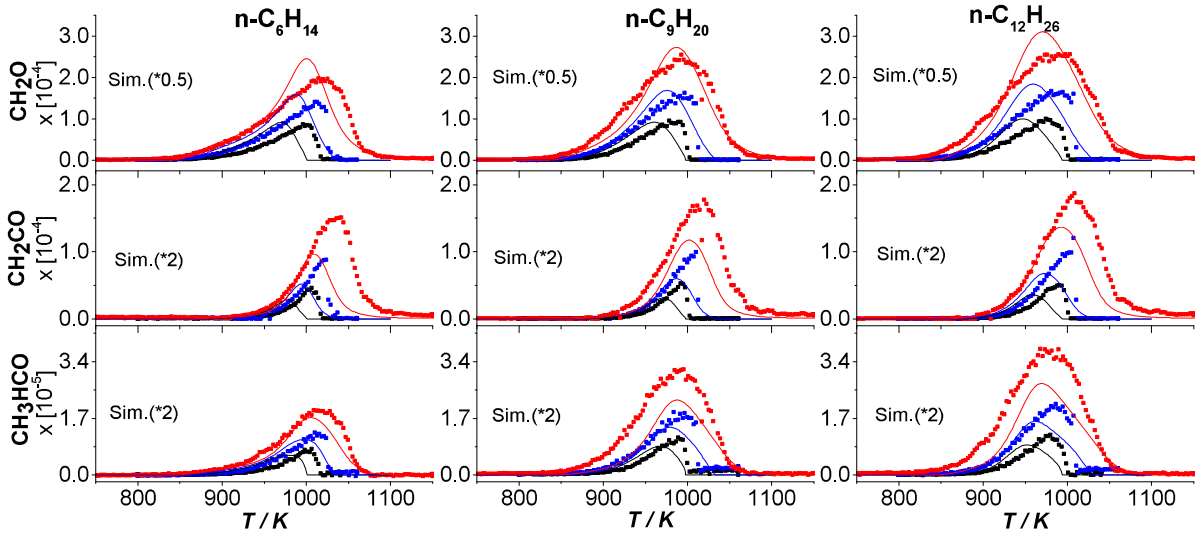

Fig. 4: Mole fraction profiles of major oxygenates as a function of oven temperatures for the three fuels studied and Φ = 0.5, 1.0, and 2.0. Symbols represent experimental data and lines modeling results. Legend: Φ = 0.5 (black), 1.0 (blue), 2.0 (red).

4.4 Olefins - Intermediates C_2 to C_{12}

Figures 5 and 6 show the measured olefins compared to the model as a function of fuel and fuel stoichiometry. With increase in the carbon number, more unsaturated species such as olefins or aromatics are produced due to a lesser hydrogen availability and enhanced total carbon content of the respective experimental conditions. This trend is visible in general from the Fig. 5 (C_2-C_6 olefins) and Fig. 6 (C_7-C_{12} olefins). The modeled results are in excellent quantitative agreement with the measurements except that for C_3H_6, C_4H_8, and $C_{10}H_{20}$. For a direct qualitative comparison of profile shapes, the modeled C_3H_6 and C_4H_8 profiles are multiplied by a factor of 3 whereas the $C_{10}H_{20}$ is multiplied by a factor of 0.5. Here, in all cases the fuel stoichiometry dependence of the fuel is in excellent agreement with the measurements.

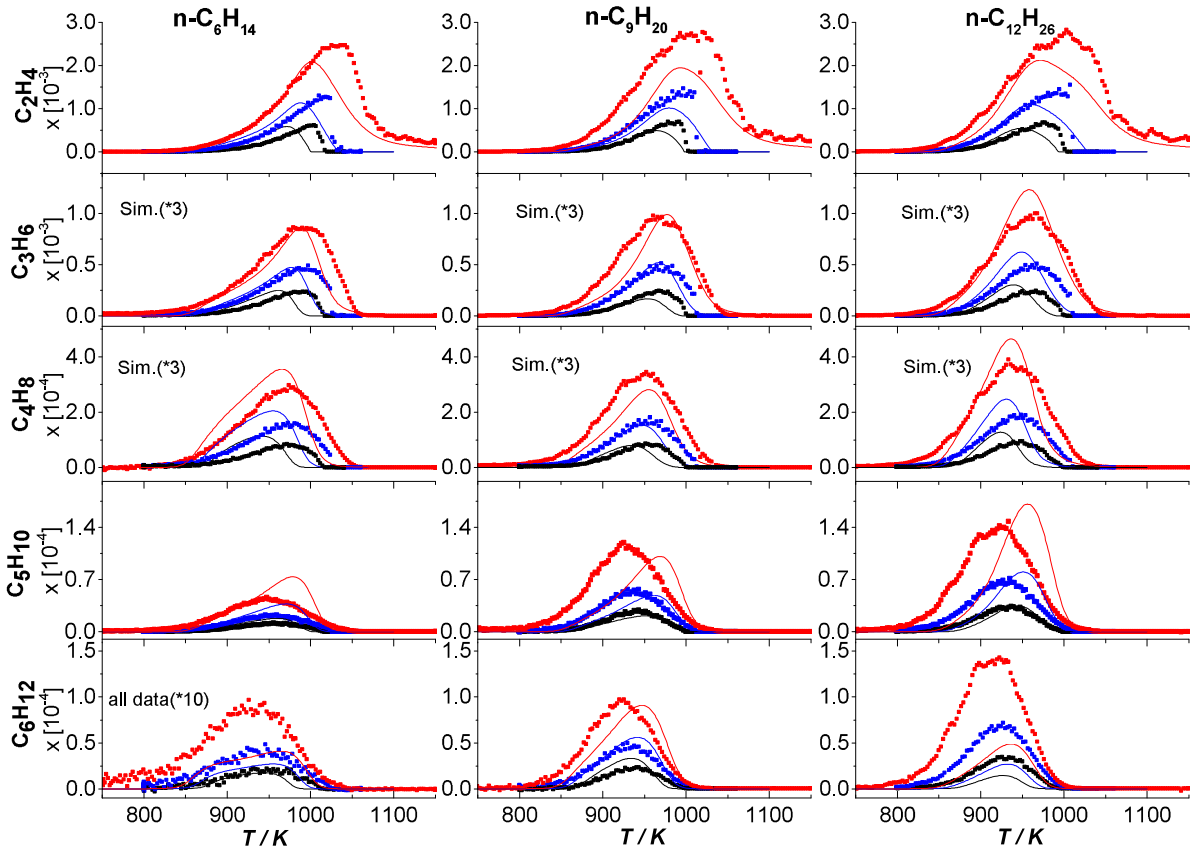

Fig. 5: Mole fraction profiles of olefins (C_2-C_6) as a function of the oven temperatures for the three fuels studied and Φ = 0.5, 1.0, and 2.0. Symbols represent experimental data and lines modeling results. Legend: Φ = 0.5 (black), 1.0 (blue), 2.0 (red).

When comparing the three fuels for the small olefins C_2H_4, C_3H_6, and C_4H_8, their maximum mole fractions are nearly independent of the initial fuel carbon number at a given stoichiometry. At a given stoichiometry, the maximum concentrations of the olefins larger than C_4 increase with increasing fuel carbon number. Few modeled species show under prediction of the fuel dependence trend. For example, the hexene (C_6H_{12}) mole fractions are well produced for n-nonane but are under-predicted by both n-hexane and n-dodecane oxidation (Fig. 5). This can be attributed to the fact that in the modeled C_6H_{12} is one of the major products of n-nonane decomposition (s. Fig. 2), whereas less than 10% C_6H_{12} is formed from n-hexane and n-dodecane decomposition. This implies the branching rate

coefficient of C_6H_{13} and $C_{12}H_{25}$ ß-scission reactions needs revision. Since these reaction rates are based on the analogy of smaller species as no real measurement or estimations are available for larger hydrocarbon this can be considered as uncertainty related to rate coefficients. Similarly the C_7, C_8, and C_9 olefins are under-predicted in n-nonane but are well reproduced for n-dodecane (Fig. 6). These olefins are not detected in the n-hexane measurements.

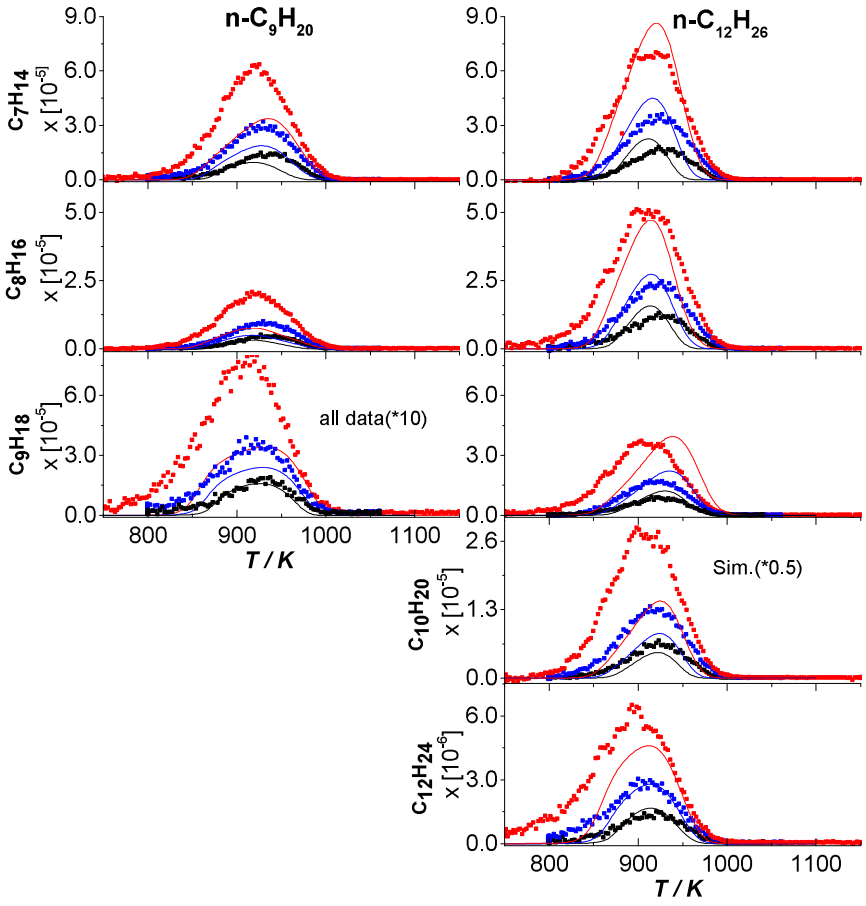

Fig. 6: Mole fraction profiles of olefins (C_7 - C_{12}) as a function of the oven temperatures for the three fuels studied and Φ = 0.5, 1.0, and 2.0. Symbols represent experimental data and lines modeling results. Legend: Φ = 0.5 (black), 1.0 (blue), 2.0 (red).

4.5 Benzene formation at different temperatures

A literature review shows that benzene can be formed in different reactions routes in different temperature regimes [23-27, 79, 80] independent of the fuel structural dependence. To understand this, the regions of temperatures can be divided into two: low- to mid-temperatures (≤ 1200 K) and high-temperatures (> 1200 K).

As discussed earlier, flame studies feature the high temperature regime with benzene formation dominantly from propargyl recombination for most fuel structures (see Table 1s in the supplemental material). The reason behind this dominance is that propargyl radicals possess exceptional high thermal and chemical stability (resonance stabilization energy 50 kJ/mol) and exhibit low reactivity towards O_2 leading to their high concentrations at flame conditions [19, 78].

Compared to this, the low- to mid-temperature benzene formation shows dominance of C_2 + C_4 reaction routes. Only a few studies discussed benzene formation in this regime:

- Pyrolysis in flow reactor have shown that at T < 1200 K, the cracking of hydrocarbons leads to acetylene formation which then polymerizes through a molecular channel to hydrocarbon mostly larger than C_4H_4 [27, 79, 80]. The acetylene polymerizes through the $2C_2H_2 \rightarrow C_4H_4$ reaction because at those temperatures the reaction $2C_2H_2 \rightarrow C_4H_3 + H$ is about 10^4 times slower [80]. Further, vinyl-acetylene and acetylene through the molecular channel form benzene ($C_4H_4 + C_2H_2 \rightarrow C_6H_6$). The possibility of this reaction is due to the concerted molecular process of triple bond to double bond addition leading to ring closure [27]. This process is so fast that the intermediate cannot be intercepted by free radical scavengers [27]. This finding also applies to oxidation.
- Recently, Nakamura et al. [26] in a micro-flow reactor at T < 1300 K, showed stronger temperature dependence of benzene compared to PAHs in a rich acetylene-

air mixture. Their modeled reaction sequence was C_2H_2 → C_4H_4→ n-C_4H_5/i-C_4H_5 + C_2H_2 → C_6H_6.

- Dagaut and Cathonnet [24] showed the fuel structure dependence on benzene formation in JSR from various unsaturated hydrocarbon fuels (C_2H_2, C_3H_4, C_3H_6, C_4H_6). In their mid-to-low temperature (900 - 1300 K) experiments, they showed the benzene formation tendency in the order $C_2H_2 < C_4H_6 < C_3H_6 < C_3H_4$.
- This trend was also seen by Rasmussen et al. [23] who measured benzene in various CH_4 flow reactor experiments doped with C_2H_2, C_2H_4, C_2H_6, C_3H_4, and C_4H_6 for high (>1400 K) and mid-to-low (1000 - 1300 K) temperatures. They found that even at low temperatures, benzene was formed directly from fuel C_3H_4 or C_4H_6 whereas no benzene was formed for CH_4 doped with C_2H_6 or C_2H_4.
- Similarly acetylene oxidation in a jet-stirred reactor study [25] showed benzene mainly formed through the $C_2 + C_4$ channel (C_2H_2 + i-C_4H_5 → fulvene → benzene) at $T < 1000$ K whereas the $C_1 + C_5$ channel was the dominant route for $T > 1000$ K. Here the authors compared seven well known literature mechanisms for C_6H_6 prediction, most of them deviated with the measurements.

These investigations point out that at least at low flame temperatures, the reaction routes to benzene formation differ from the widely accepted propargyl radicals' reaction at flame conditions and support the $C_2 + C_4$ route as dominant benzene formation channel. Unfortunately, all these investigations are only available for fuels with less than 5 carbon atoms.

Relevant to this study, the $C_2 + C_4$ benzene formation reactions in the mechanism of present work are: n-C_4H_5 + C_2H_3 → C_6H_6 + H_2, n-C_4H_5 + C_2H_2 → C_6H_6 + H, i-C_4H_5 + C_2H_4 → C_6H_6 + H + H_2, i-C_4H_5 + C_2H_2 → C_6H_6 + H, and i-C_4H_5 + C_2H → C_6H_6. In addition, reactions of fulvene added to the mechanism are: i-C_4H_5 + C_2H_2 = fulvene + H, n-C_4H_5 +

C_2H_2 = fulvene + H, C_5H_5 + CH_3 = fulvene + 2H, C_3H_3 + C_3H_3 = fulvene, C_3H_3 + C_3H_5 = fulvene + 2H, fulvene = C_6H_5 + H, fulvene = C_6H_6, and fulvene + H = C_6H_6 + H.

Predictions of benzene for the three n-alkanes studied in this work are shown in the Fig. 7(left). The figure shows a comparison of the measured and predicted benzene mole fraction for all the three fuels. Here, it should be noted that all the predicted profiles are multiplied by factor of 2.5. The profile shapes are well reproduced by the mechanism and considering the measurement uncertainty of 50% for this measurement and uncertainties in rate constants of modeled benzene precursors, this can still be considered a reasonable result. A relative comparison in Fig. 7(right) shows, with increase in carbon number and fuel stoichiometry, the benzene formation increases, which is apparent.

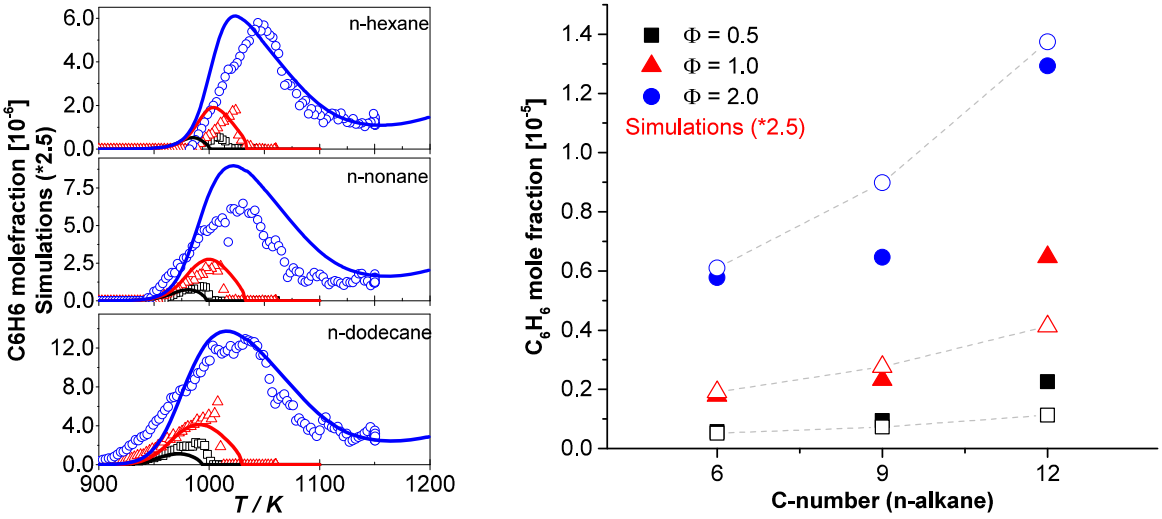

Fig. 7: Benzene profiles and maximum mole fraction for the three fuels studied and Φ = 0.5 (black), 1.0 (red), and 2.0 (blue). Symbols represent experimental data and lines modeling results. Dotted lines in the right figure are only guiding lines.

The influence of the fuel itself on benzene formation can be seen from the decomposition of the first fuel radical. In case of n-dodecane, the fuel radical ($sC_{12}H_{25}$, sec-dodecyl radical) decomposes to form C_4H_8 in the reaction $sC_{12}H_{25}$ → pC_8H_{17} + C_4H_8. Similarly, in n-hexane and n-nonane the fuel radicals s-C_6H_{13} and s-C_9H_{19}, respectively, decompose to give C_4H_8. In

all cases, the C_4H_8 leads to benzene formation through C_4H_8 → nC_4H_7 → nC_4H_6 → $i\text{-}C_4H_5$ → C_6H_6 pathways.

The model prediction of benzene precursors are compared in Figure 8. The C_2H_4 and C_2H_2 are involved in the reactions with C_4H_6 and C_4H_8 to form benzene. The comparison of the model prediction with the respective experiments shows that the model in general is capable to reproduce increasing trend with stoichiometry at all temperatures. The C_2H_2 profiles in rich case (Φ = 2.0) presents a small region of plateau between two distinct regions of maxima. The second increase is not reproduced by our model to the extent of measurement. Among the literature mechanisms only POLIMI reproduce the second measured increase. At these temperatures acetylene is mainly consumed to form C_2H_3, which is similar to our mechanism. Interestingly for other fuels, we observed similar results where C_2H_2 profile (at rich conditions) in intermediate regime is typically in excellent agreement while the rise at the high temperature often deviates significantly by the model (up to a factor 2-3) [62, 63]. Thus, the under-prediction of C_2H_2 at high temperature owing to very limited knowledge about this regime remains unclear. The simulated maximum mole fractions of C_4H_6 and C_4H_8 are under-predicted by factor of 2 and 3 respectively which can be responsible for under prediction of benzene formation. Here, the measurement uncertainties of these two species are about 30%.

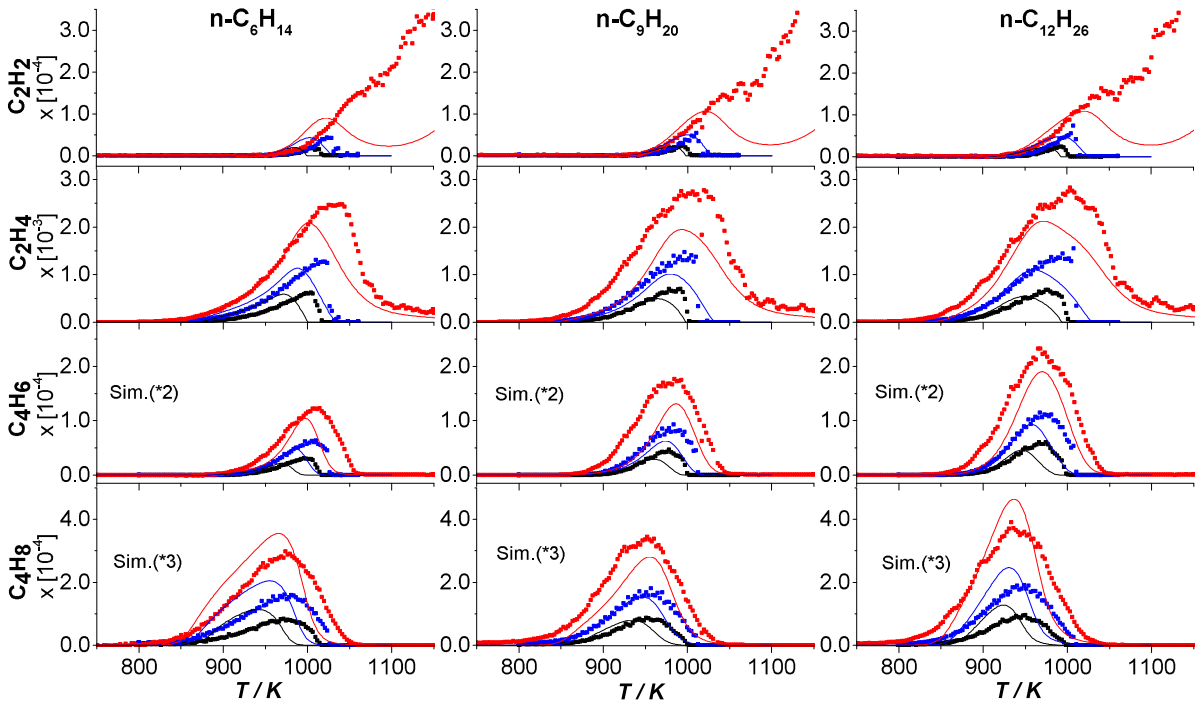

Fig. 8: Mole fraction profiles of benzene and benzene precursors as a function of the oven temperature for the three fuels studied and Φ = 0.5, 1.0, and 2.0. Symbols represent experimental data and lines modeling results. Legend: Φ = 0.5 (black), 1.0 (blue), 2.0 (red).

The predictions of benzene formation by literature reaction mechanisms are compared in Fig. 9. The mechanisms that include benzene pathways for n-dodecane are JetSurF 2.0 [44], POLIMI [50] and RWTH [77]. Only JetSurF 2.0 mechanism includes also n-hexane and n-nonane. As shown in Fig. 9 (right), all the mechanisms under-predict the measured benzene formation by factor of 3 to 15, which is striking as all these mechanisms are supposed to be optimized to predict soot precursors and therefore also benzene formation.

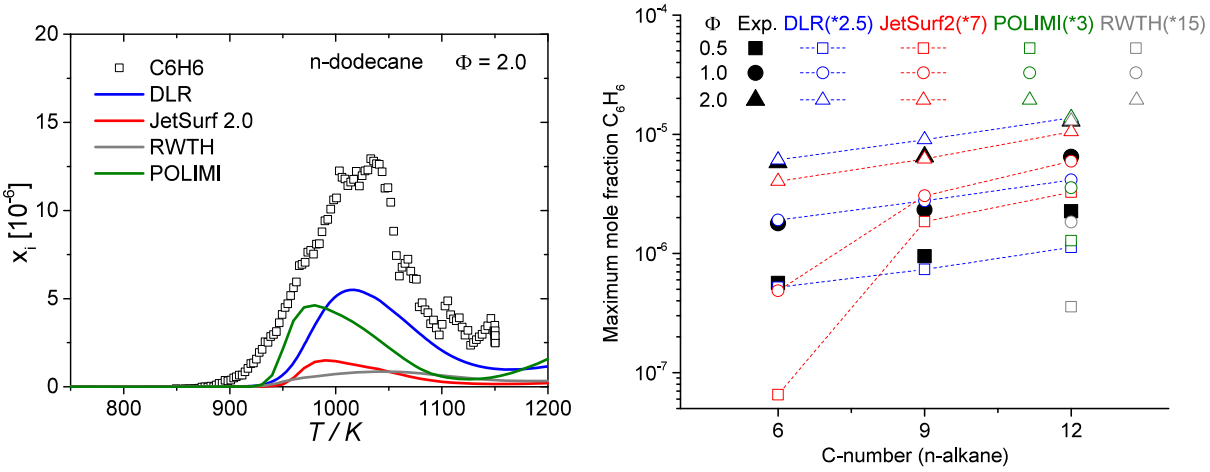

Fig. 9: Maximum benzene mole fraction for the three studied fuels and Φ = 0.5, 1.0, and 2.0. Symbols represent experimental data and lines modeling results. Dotted lines in the right figure are only guiding lines.

For the conditions of our experiments, all the above mentioned mechanisms have common benzene consumption reaction $C_6H_6 \rightarrow C_6H_5 + H$ forming phenyl and the major benzene formation reactions differ slightly:

DLR: $i\text{-}C_4H_5 + C_2H_4 \rightarrow C_6H_6 + H + H_2$ and $i\text{-}C_4H_5 + C_2H_2 \rightarrow C_6H_6 + H$

JetSurF 2.0: $C_4H_6 + C_2H_3 \rightarrow C_6H_6 + H + H_2$

POLIMI: $C_4H_{5,total} + C_2H_4 \rightarrow C_6H_6 + H + H_2$

RWTH: $i\text{-}C_4H_5 + C_2H_2 \rightarrow$ fulvene $+ H \rightarrow C_6H_6 + H$

Among the fulvene formation routes $i\text{-}C_4H_5/n\text{-}C_4H_5 + C_2H_2 \rightarrow$ fulvene + H, $C_5H_5 + CH_3 \rightarrow$ fulvene, $C_3H_3 + C_3H_3 \rightarrow$ fulvene, $C_3H_3 + C_3H_5 \rightarrow$ fulvene, the latter three are unimportant for present conditions due to nearly zero mole fractions ($<10^{-8}$) of corresponding radicals required for its formation. Insertion of above reactions leads to benzene formation via fulvene (by H-assisted conversion) by <0.1% (at 50% benzene formation for all fuels and stoichiometries studied). The major channel remains $i\text{-}C_4H_5 + C_2H_4$ (and C_2H_2) $\rightarrow C_6H_6$. Thus, the inclusion of fulvene has no visible effect on benzene formation.

All these mechanisms consider the C_2 + C_4 (even route) as a major benzene formation source however the species/radical itself varies. All mechanisms, except JetSurF 2.0, consider the C_4H_5 radical as the C_4-species governing benzene formation. Theoretical studies and direct measurements in flames have shown that i-C_4H_5 isomer is more abundant than n-C_4H_5 as a result of resonance stabilization [55] due to which the thermochemistry favors formation of the i-C_4H_5 isomer. This is reflected by our model where the concentration of i-C_4H_5 is about two orders larger than that of n-C_4H_5. The rate coefficient of n-C_4H_5 + C_2H_x → C_6H_6 (x = 2, 3, 4) is significantly larger than that of the i-C_4H_5 isomer but due to low concentration of n-C_4H_5, the contribution towards benzene formation is dominated by i-C_4H_5, which was also pointed out in Senosiain and Miller [81]. The reaction rates of benzene formation reactions as well as concentration of benzene precursor species varies among the mechanisms discussed above leading to the scatter in benzene formation predictions. Analysis of the DLR mechanism shows that the benzene formation is dominated by the reactions of i-C_4H_5 + C_2H_4 → C_6H_6 + H + H_2 and i-C_4H_5 + C_2H_2 → C_6H_6 + H, their relative importance being dependent on the temperatures at which C_2H_4 and C_2H_2 is formed. It appears that the absence of either or both of these two reactions in JetSurF 2.0 and RWTH models leads to noticeably lesser contribution to benzene formation giving maximum deviation observed with the measurements. For the DLR and POLIMI models where benzene predictions are close to the experiments, these two reactions are present.

Compared to the benzene predictions at the flow reactor conditions, the agreement in predictions by these mechanisms in flames is better. For example, benzene is measured by Doute et al. [82] in an atmospheric laminar premixed decane-air flame at rich condition (Φ = 1.7). The benzene formation reaction at flame temperatures is dominantly the propargyl recombination reaction ($2C_3H_3$ → C_6H_6). For this case the benzene mole fraction varies up to a factor of 2 compared to measurements (see Fig. 10) but still by a factor of 4 among each

other. At $T < 1100$ K, the propargyl concentrations are as low as 10^{-8} (e.g. in n-dodecane, Φ = 2.0) whereas at flame temperatures, the propargyl mole fraction is about 10^{-4} (e.g. in n-decane-air flame, Φ = 1.7). Thus, propargyl concentrations are not sufficient to form benzene at lower temperatures typical to flow reactor experiments. Though in flames, lower temperature condition do exists closer to the burner surface. However, measurement uncertainties are very high at low flame positions. The influence of small species chemistry on benzene formation cannot be verified based on present flame experiment.

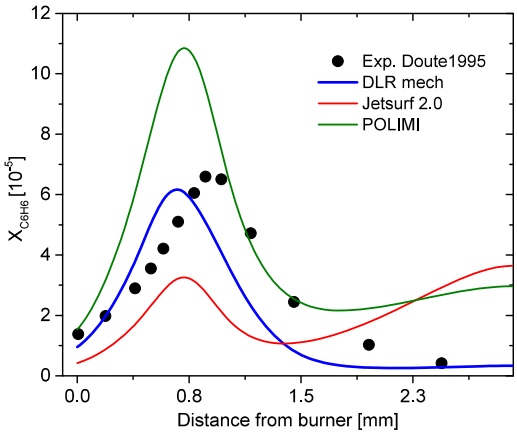

Fig. 10: Benzene mole fractions in an atmospheric laminar premixed decane-air flame at Φ = 1.7. Experiments: symbol [82], lines: simulations.

To extend the above discussion on how the $C_2 + C_4$ route correlates to the benzene formation at low flow reactor temperatures, we plotted various precursor species against benzene. In Figure 11, the maximum benzene mole fractions are plotted against the maxima of various precursor species for all fuels and stoichiometries investigated in the present work. Here, both simulated and measured (when available) mole fractions are plotted. For the fuels studied in this work, the benzene formation in the simulations follows the route: Fuel → first fuel radical → nC_4H_8 → nC_4H_7 → C_4H_6 → $i\text{-}C_4H_5$ → C_6H_6. Along with these species, C_2H_2 and C_2H_4 are important as they react with $i\text{-}C_4H_5$ to form benzene. The plot shows that the maximum mole fractions of C_2H_2, C_2H_4, C_4H_6, and C_4H_8 correlate very well with the

maximum benzene mole fractions for all the three stoichiometries and three fuels studied. This observation is supported by both experiments and simulations. The simulated i-C_4H_5 radical, which is not measured, shows also linear fit to the maximum benzene concentration. The propargyl radical C_3H_3 shows no correlation with benzene.

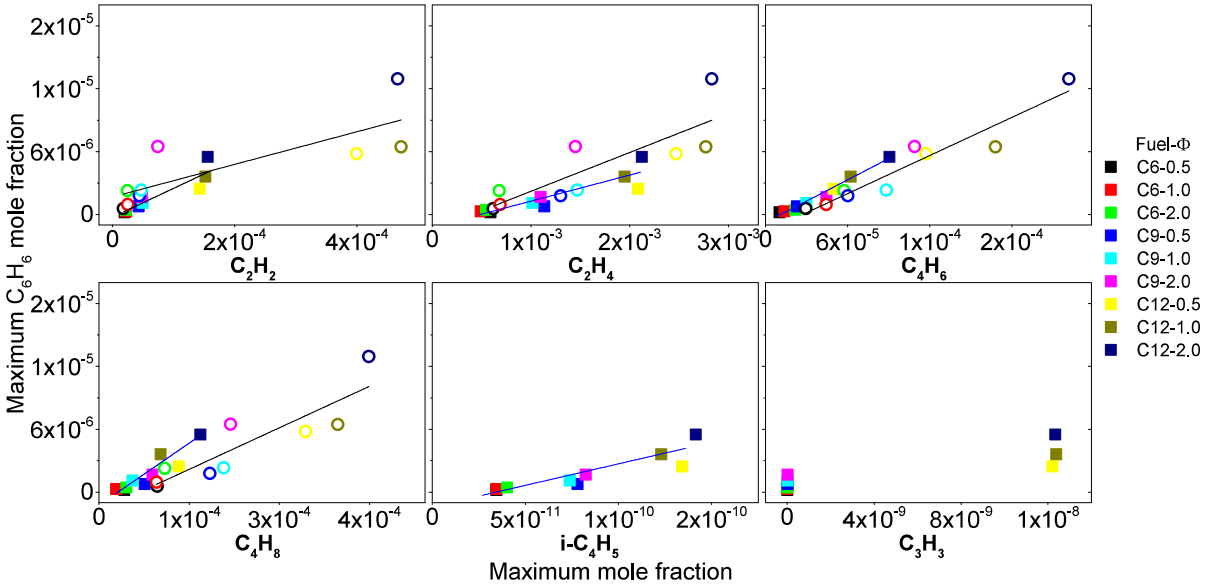

Fig. 11: Maximum benzene concentrations are plotted against various C_2 - C_4 stable species and radicals considered important precursors to benzene formation. Both experiments (circle) and simulations (square) are plotted for all three fuels and stoichiometries. An increase in benzene mole fraction to increase in precursor mole fraction is shown by a fitting line.

The benzene formations at intermediate temperature do vary from high flame temperature routes. The focus of present work has been restricted to n-alkanes only and the influence of C_2 + C_4 route may vary for other reaction classes. At this point, we cannot state a general dominance for C_2 + C_4 benzene formation route at intermediate temperatures beyond the investigated n-alkanes. For this reason a general conclusion for benzene formation pathways in the intermediate temperature range is not feasible from this study alone and the present

results should be considered as an observation proofing the need for future studies of other fuel classes.

5. Conclusion

Reaction kinetics of three n-alkanes is investigated in this work as a representative of larger n-alkanes that can be found in the continuous distribution of n-alkanes in FT processes. This study intends to investigate larger hydrocarbons for their variation in carbon number and fuel stoichiometry at lower end of temperatures relevant for technical combustors. The reaction kinetics is investigated to obtain species spectrum produced by the fuel and to understand the reaction routes of benzene formation. A DLR high temperature flow reactor setup with coupled MBMS detection system is employed to obtain speciation data for the above stated fuels. Speciation data of n-hexane, n-nonane, and n-dodecane are studied in an atmospheric flow reactor for three different equivalence ratios (Φ = 0.5, 1.0, and 2.0). A detailed reaction model succeeds in reproducing all the measured species and is in good agreement with the measurements. Both the measurement and simulations provide insight into major reaction pathways as well as into the product spectrum and prediction of soot precursors during the oxidation of the three fuels studied. Since the flow reactor is operated at temperatures comparable to intermediate flame temperature (in this case below 1200 K), reaction pathways leading to benzene in n-alkanes are found to be formed from the C_2 + C_4 route unlike in flames (T > 1400 K), where propargyl recombination is important. Most of the literature mechanisms are found not optimal to predict benzene formation at such temperatures. In this work, only n-alkanes are studied, therefore the influence of C_2 + C_4 route cannot be verified for other reaction classes. However, it emphasizes the need for understanding benzene formation at intermediate flame temperature, which usually occurs in the lower temperature zones of practical combustion devices.

6. Acknowledgements

The authors gratefully acknowledge the support of Helmholtz Association for funding the project SynKWS (Synthetic liquid hydrocarbons) and German Aerospace Center (Deutsches Zentrum für Luft- und Raumfahrt, DLR) internal project ECLIF (Emission and Climate Impact of Alternative Fuels). The results related to n-alkanes are part of SynKWS whereas the benzene study is undertaken within ECLIF. P.O. and M.K. thank Larissa Kracht for her assistance with the measurements. The authors gratefully acknowledge funding by the German Federal Ministry of Education and Research (BMBF) within the Kopernikus Project P2X.

7. References

[1] S. Chu, A. Majumdar, Opportunities and challenges for a sustainable energy future, Nature 488 (2012) 294–303.

[2] W.M. Verdegaal, S. Becker, C. von Olshausen, Power-to-liquids: synthetic crude oil from CO2, water, and sunshine, Chem. Ing. Tech. 87 (2015) 340–346.

[3] M. Moser, T. Pregger, S. Simon, D. König, A. Wörner, R.-U. Dietrich, M. Köhler, P. Oßwald, J. Grohmann, T. Kathrotia, G. Eckel, D. Schweitzer, N. Armbrust, H. Dieter, G. Scheffknecht, C.Kern, J. Thiessen, A. Jess, M. Aigner, Synthetische flüssige Kohlenwasserstoffe aus erneuerbaren Energien – Ergebnisse der Helmholtz Energieallianz. Chem. Ing. Tech. 89 (2017) 274–288. doi:10.1002/cite.201500154.

[4] G. Schaub, R. Edzang, Synthetic fuels from natural gas and biomass - status and perspectives, Chem. Ing. Tech. 83 (2011) 1912–1924.

[5] IATA 2014 Report on alternative fuels, December 2014, ISBN 978-92-9252-508-8

[6] N. Marinov, W.J. Pitz, C.K. Westbrook, A.M. Vincitore, M.J. Castaldi, S.M. Senkan, C. F. Melius, Aromatic and polycyclic aromatic hydrocarbon formation in a laminar premixed n-Butane flame, Combust. Flame 114 (1998) 192–213.

[7] C.J. Pope, J.A. Miller, Exploring old and new benzene formation pathways in low-pressure premixed flames of aliphatic fuels, Proc. Combust. Inst. 28 (2000) 1519–1527.

[8] A. Lamprecht, B. Atakan and K. Kohse-Hoeinghaus, Fuel-rich flame chemistry in low-pressure cyclopentene flames, Proc. Combust. Inst. 28 (2000) 1817–1824.

[9] N. Hansen, J.A. Miller, C.A. Taatjes, J. Wang, T.A. Cool, M.E. Law, P.R. Westmoreland, Photoionization mass spectrometric studies and modeling of fuel-rich allene and propyne flames, Proc. Combust. Inst. 31 (2007) 1157–1164.

[10] N. Hansen, T. Kasper, S.J. Klippenstein, P.R. Westmoreland, M.E. Law, C.A. Taatjes, K. Kohse-Höinghaus, J. Wang, T.A. Cool, Initial steps of aromatic ring formation in a laminar premixed fuel-rich cyclopentene flame, J. Phys. Chem. A 111 (2007) 4081–4092.

[11] M.E. Law, P.R. Westmoreland, T.A. Cool, J. Wang, N. Hansen, C.A. Taatjes, T. Kasper, Benzene precursors and formation routes in a stoichiometric cyclohexane flame, Proc. Combust. Inst. 31 (2007) 565–573.

[12] H.R. Zhang, E.G. Eddings, A.F. Sarofim, C.K. Westbrook, Fuel dependence of benzene pathways, Proc. Combust. Inst. 32 (2009) 377–385.

[13] N. Hansen, J.A. Miller, P.R. Westmoreland, T. Kasper, K. Kohse-Hoeinghaus, J. Wang, T.A. Cool, Isomer-specific combustion chemistry in allene and propyne flames, Combust. Flame 156 (2009) 2153–2164.

[14] N. Hansen, J.A. Miller, T. Kasper, K. Kohse-Hoeinghaus, P.R. Westmoreland, J. Wang, T.A. Cool, Benzene formation in premixed fuel-rich 1,3-butadiene flames, Proc. Combust. Inst. 32 (2009) 623–630.

[15] N.A. Slavinskaya, P. Frank, A modelling study of aromatic soot precursors formation in laminar methane and ethene flames, Combust. Flame 156 (2009) 1705–1722.

[16] N. Hansen, T. Kasper, B. Yang, T.A. Cool, W. Li, P.R. Westmoreland, P. Oßwald, K. Kohse-Hoeinghaus, Fuel-structure dependence of benzene formation processes in premixed flames fueled by C6H12 isomers, Proc. Combust. Inst. 33 (2011) 585–592.

[17] W. Li, M.E. Law, P.R. Westmoreland, T. Kasper, N. Hansen, K. Kohse-Hoeinghaus, Multiple benzene-formation paths in a fuel-rich cyclohexane flame, Combust. Flame 158 (2011) 2077–2089.

[18] H. Jin, A. Frassoldati, Y. Wang, X. Zhang, M. Zeng, Y. Li, F. Qi, A. Cuoci, T. Faravelli, Kinetic modeling study of benzene and PAH formation in laminar methane flames, Combust. Flame 162 (2015) 1692–1711.

[19] R.X. Fernandes, H. Hippler, M. Olzmann, Determination of the rate coefficient for the C3H3+C3H3 reaction at high temperatures by shock-tube investigations, Proc. Combust. Inst. 30 (2005) 1033–1038.

[20] K.P. Geigle, W. O'Loughlin, R. Hadef, W. Meier, Visualization of soot inception in turbulent pressurized flames by simultaneous measurement of laser-induced fluorescence of polycyclic aromatic hydrocarbons and laser-induced incandescence, and correlation to OH distributions, Appl. Phys. B 119 (2015) 717–730.

[21] K.P. Geigle, M. Köhler, W. O'Loughlin, W. Meier, Investigation of soot formation in pressurized swirl flames by laser measurements of temperature, flame structures and soot concentrations, Proc. Combust. Inst. 35 (2015) 3373–3380.

[22] C. Eberle, P. Gerlinger, K.P. Geigle, M. Aigner, Numerical investigation of transient soot evolution processes in an aero-engine model combustor, Combust. Sci. Technol. 187 (2015) 1841–1866.

[23] M.S. Skjøth-Rasmussen, P. Glarborg, M. Østberg, M.B. Larsen, S.W. Sørensen, J.E. Johnsson, A.D. Jensen, T.S. Christensen, A study of benzene formation in a laminar flow reactor, Proc. Combust. Inst. 29 (2002) 1329–1336.

[24] P. Dagaut M. Cathonnet, A comparative study of the kinetics of benzene formation from unsaturated C2 to C4 hydrocarbons, Brief Communication, Combust. Flame 113 (1998) 620–623.

[25] B. Wang, Y. Liu, J. Weng, P. Glarborg, Z. Tian, New insights in the low-temperature oxidation of acetylene, Proc. Combust. Inst. 36 (2017) 355–363.

[26] H. Nakamura, R. Tanimoto, T. Tezuka, S. Hasegawa, K. Maruta, Soot formation characteristics and PAH formation process in a micro flow reactor with a controlled temperature profile, Combust. Flame 161 (2014) 582–591.

[27] C. Chanmugathas, J. Heicklen, Pyrolysis of acetylene vinylacetylene, Mixtures between 400 and 500°C, Int. J. Chem. Kinet. 18 (1986) 701–718.

[28] V.P. Zhukov, V.A. Sechenov, A. Starikovskii, Ignition delay times in lean n-hexane–air mixture at high pressures, Brief Communications, Combust. Flame 136 (2004) 257–259.

[29] D.F. Davidson and R.K. Hanson, Fundamental kinetics database utilizing shock tube measurements volume 4: ignition delay time measurements (Jan. 2005 to Jan. 2014), page 30.

[30] K. Zhang, C. Banyon, C. Togbe, P. Dagaut, J. Bugler, H.J. Curran, An experimental and kinetic modeling study of n-hexane oxidation, Combust. Flame 162 (2015) 4194–4207.

[31] B. Rotavera, P. Dievart, C. Togbe, P. Dagaut, E.L. Petersen, Oxidation kinetics of n-nonane: Measurements and modeling of ignition delay times and product concentrations, Proc. Combust. Inst. 33 (2011) 175–183.

[32] J. He, K. Yong, W. Zhang, P. Li, C. Zhang, X. Li, Shock tube study of ignition delay characteristics of n-nonane and n-undecane in argon, Energ. Fuel 30 (2016) 8886−8895.

[33] H.S. Shen, J. Steinberg, J. Vanderover, M.A. Oehlschlaeger, A shock tube study of the ignition of n-heptane, n-decane, n-dodecane, and n-tetradecane at elevated pressures, Energ. Fuel 23 (2009) 2482–2489.

[34] S.S. Vasu, D.F. Davidson, Z. Hong, V. Vasudevan, R.K. Hanson, n-Dodecane oxidation at high-pressures: Measurements of ignition delay times and OH concentration time-histories, Proc. Combust. Inst. 32 (2009) 173–180.

[35] D.R. Haylett, D.F. Davidson, R.K. Hanson, Ignition delay times of low-vapor-pressure fuels measured using an aerosol shock tube, Combust. Flame 159 (2012) 552–561.

[36] D.F. Davidson, Z. Hong, G.L. Pilla, A. Farooq, R.D. Cook, R.K. Hanson, Multi-species time-history measurements during n-dodecane oxidation behind reflected shock waves, Proc. Combust. Inst. 33 (2011) 151–157.

[37] T. Malewicki, K. Brezinsky, Experimental and modeling study on the pyrolysis and oxidation of n-decane and n-dodecane, Proc. Combust. Inst. 34 (2013) 361–368.

[38] C. Ji, E. Dames, Y.L. Wang, H. Wang, F.N. Egolfopoulos, Propagation and extinction of premixed C5 –C12 n-alkane flames, Combust. Flame 157 (2010) 277–287.

[39] S. Coronel, R. Mevel, N. Chaumeix, P. Vervish, P. A. Boettcher, V. Thomas, N. Darabiha, J. E. Shepherd, Laminar burning speed of n-hexane-air mixtures, 8th US National Combustion Meeting WSSCI, University of Utah May 19-22, 2013, Paper # 070LT-0383.

[40] K. Kumar C. Sung, Flame propagation and extinction characteristics of neat surrogate fuel components, Energ. Fuel 24 (2010) 3840–3849.

[41] A.P. Kelley, A.J. Smallbone, D. Zhu, C.K. Law, Laminar flame speeds of C5 to C8 n-alkanes at elevated pressures and temperatures, 48th AIAA Aerospace Sciences Meetings (2010), AIAA 2010-774.

[42] Z. Wang, O. Herbinet, Z.Cheng, B. Husson, E. Fournet, F. Qi, F. Battin-Leclerc, Experimental investigation of the low temperature oxidation of the five isomers of hexane, J. Phys. Chem. A 118 (2014) 5573−5594.

[43] A. Mze-Ahmed, K. Hadj-Ali, P. Dagaut, G. Dayma, Experimental and modeling study of the oxidation kinetics of n-undecane and n-dodecane in a jet-stirred reactor, Energ. Fuel 26 (2012) 4253−4268.

[44] H. Wang, E. Dames, B. Sirjean, D. A. Sheen, R. Tango, A. Violi, J.Y. W. Lai, F.N. Egolfopoulos, D.F. Davidson, R.K. Hanson, C.T. Bowman, C.K. Law, W. Tsang, N.P. Cernansky, D.L. Miller, R.P. Lindstedt, A high-temperature chemical kinetic model of n-alkane (up to n-dodecane), cyclohexane, and methyl-, ethyl-, n-propyl and n-butyl-cyclohexane oxidation at high temperatures, JetSurF 2.0, Sept. 19, 2010 (http://melchior.usc.edu/JetSurF/JetSurF2.0).

[45] H.P. Ramirez, K. Hadj-Ali, P. Dievart, G. Dayma, C. Togbe, G. Moreac, P. Dagaut, Oxidation of commercial and surrogate bio-Diesel fuels (B30) in a jet-stirred reactor at elevated pressure: Experimental and modeling kinetic study, Proc. Combust. Inst. 33 (2011) 375–382.

[46] G. Blanquart, P. Pepiot-Desjardins, H. Pitsch, Chemical mechanism for high temperature combustion of engine relevant fuels with emphasis on soot precursors, Combust. Flame 156 (2009) 588–607.

[47] S.M. Sarathy, M. Mehl, C. K. Westbrook, W. J. Pitz,C. Togbe, P. Dagaut, H. Wang, M.A. Oehlschlaeger, U. Niemann, K. Seshadri,P.S. Veloo, C. Ji, F.N. Egolfopoulos, T. Lu, Comprehensive chemical kinetic modeling of the oxidation of 2-methylalkanes from C7 to C20, Combust. Flame 158 (2011) 2338–2357.

[48] B. Rotavera, E.L. Petersen, Ignition behavior of pure and blended methyl octanoate, n-nonane, and methylcyclohexane, Proc. Combust. Inst. 34 (2013) 435–442.

[49] S. Banerjee, R. Tangko, D.A. Sheen, H. Wang, C.T. Bowman, An experimental and kinetic modeling study of n-dodecane pyrolysis and oxidation, Combust. Flame 163 (2016) 12–30.

[50] E. Ranzi, CRECK Modeling Group, Mechanism of Real Transportation Fuels, Primary Reference Fuels (PRF) + PAH + Real Fuels, Ver. 1412, Dec. 2014, http://creckmodeling.chem.polimi.it/.

[51] N. Hansen, M. Schenk, K. Moshammer, K. Kohse-Höinghaus, Investigating repetitive reaction pathways for the formation of polycyclic aromatic hydrocarbons in combustion processes, Combust. Flame 180 (2017) 250–261.

[52] Y. Wang, A. Makwana, S. Iyer, M. Linevsky, R.J. Santoro, T.A. Litzinger, J. O'Connor, Effect of fuel composition on soot and aromatic species distributions in laminar, co-flow flames. Part 1. Non-premixed fuel, Combust. Flame 189 (2018) 443–455.

[53] M. Koehler, T. Kathrotia, P. Osswald, M. Fischer-Tammer, K. Moshammer, U. Riedel, 1-, 2- and 3-pentanol combustion in laminar hydrogen flames - a comparative experimental and modeling study, Combust. Flame 162 (2015) 3197–3209.

[54] A.W. Jasper, N. Hansen, Hydrogen-assisted isomerizations of fulvene to benzene and of larger cyclic aromatic hydrocarbons, Proc. Combust. Inst. 34 (2013) 279–287.

[55] N. Hansen, T.A. Cool, P.R. Westmoreland, K. Kohse-Hoeinghaus, Recent contributions of flame-sampling molecular-beam mass spectrometry to a fundamental understanding of combustion chemistry, Prog. Energ. Combust. Sci. 35 (2009) 168–191.

[56] J. Miller, S. Klippenstein, Y. Georgievskii, L.B. Harding, W. Allen, A. Simmonett, Reactions between resonance-stabilized radicals: Propargyl+Allyl, J. Phys. Chem. A 114 (2010), 4881–4890.

[57] N. Marinov, M.J. Castaldi, C. F. Melius, W. Tsang, Aromatic and polycyclic aromatic hydrocarbon formation in a premixed propane flame, Combust. Sci. Technol. 128 (1997) 295–342, doi:10.1080/00102209708935714.

[58] Y. Georgievskii, J.A. Miller, S. Klippenstein, Association rate constants for reactions between resonance-stabilized radicals: C_3H_3+C_3H_3, C_3H_3+C_3H_5, and C_3H_5+C_3H_5, Phys. Chem. Chem. Phys. 9 (2007) 4259–4268.

[59] P. Oßwald, M. Köhler, An atmospheric pressure high-temperature laminar flow reactor for investigation of combustion and related gas phase reaction systems, Rev. Sci. Instrum. 86 (2015) 105–109.

[60] P. Oßwald, R. Whitside, J. Schäffer, M. Köhler, An experimental flow reactor study of the combustion kinetics of terpenoid jet fuel compounds: Farnesane, p-menthane and p-cymene, Fuel 187 (2017) 43–50.

[61] Chemical WorkBench® 4.0, Kintech Lab. (2013), http://www.kintechlab.com/products/chemical-workbench/

[62] T. Kathrotia, C. Naumann, P. Oßwald, M. Köhler, U. Riedel, Kinetics of Ethylene Glycol: The first validated reaction scheme and first measurements of ignition delay times and speciation data, Combust. Flame 179 (2017) 172–184.

[63] M. Köhler, P. Oßwald, H.-B. Xu, T. Kathrotia, C. Hasse, U. Riedel, Speciation data for fuel-rich methane oxy-combustion and reforming under prototypical partial oxidation conditions, Chem. Eng. Sci. 139 (2016) 249–260.

[64] F. Herrmann, B. Jochim, P. Oßwald, L. Cai, H. Pitsch, K. Kohse-Höinghaus, Experimental and numerical low-temperature oxidation study of ethanol and dimethyl ether, Combust. Flame 161 (2014) 384–397.

[65] P. Oßwald, P. Hemberger, T. Bierkandt, E. Akyildiz, M. Köhler, A. Bodi, T. Gerber, T. Kasper, In situ flame chemistry tracing by imaging photoelectron photoion coincidence spectroscopy, Rev. Sci. Instrum. 85 (2014) 025101, doi: 10.1063/1.4861175.

[66] J. Krueger, G.A. Garcia, D. Felsmann, K. Moshammer, A. Lackner, A. Brockhinke, L. Nahon, K. Kohse-Hoinghaus, Photoelectron-photoion coincidence spectroscopy for multiplexed detection of intermediate species in a flame, Phys. Chem. Chem. Phys. 16 (2014) 22791–22804.

[67] F. Qi, Combustion chemistry probed by synchrotron VUV photoionization mass spectrometry, Proc. Combust. Inst. 34 (2013), 33–63.

[68] N. Hansen, T.A. Cool, P.R. Westmoreland, K. Kohse-Höinghaus, Recent contributions of flame-sampling molecular-beam mass spectrometry to a fundamental understanding of combustion chemistry, Prog. Energ. Combust. Sci. 35 (2009) 168–191.

[69] P. Oßwald, H. Güldenberg, K. Kohse-Höinghaus, B. Yang, T. Yuan, F. Qi, Combustion of butanol isomers - A detailed molecular beam mass spectrometry investigation of their flame chemistry, Combust. Flame 158 (2011) 2–15, doi: 10.1016/j.combustflame.2010.06.003.

[70] M. Schenk, L. Leon, K. Moshammer, P. Oßwald, T. Zeuch, L. Seidel, F. Mauss, K. Kohse-Höinghaus, Detailed mass spectrometric and modeling study of isomeric butene flames, Combust. Flame 160 (2013) 487–503.

[71] F. Herrmann, P. Oßwald, K. Kohse-Höinghaus, Mass spectrometric investigation of the low-temperature dimethyl ether oxidation in an atmospheric pressure laminar flow reactor, Proc. Combust. Inst. 34 (2013) 771–778.

[72] J.C. Biordi, Molecular beam mass spectrometry for studying the fundamental chemistry of flames, Prog. Energ. Combust. Sci. 3 (1977) 151–173.

[73] D.A. Knyazkov, N. Slavinskaya, A. Dmitriev, A. Shmakov, O. Korobeinichev, U. Riedel, Structure of an n-heptane/toluene flame: Molecular beam mass spectrometry and computer simulation investigations, Combust Explos. Shock 52 (2016) 142–154.

[74] C.K. Westbrook, W.J. Pitz, O. Herbinet, H.J. Curran, E.J. Silke, A comprehensive detailed chemical kinetic reaction mechanism for combustion of n-alkane hydrocarbons from n-octane to n-hexadecane, Combust. Flame 156 (2009) 181–199.

[75] M. Nehse, Automatische Erstellung von detaillierten Reaktionsmechanismen zur Modellierung der Selbstzuendung und laminarer Vormisch flammen von gasformigen Kohlenwassersto –

Mischungen, Dissertation, University of Heidelberg (2001), https://www.iwr.uni-heidelberg.de/groups/reaflow/Diss/Nehse(2001).pdf

[76] D.L. Baulch, C.T. Bowman, C.J. Cobos, R.A. Cox, Th. Just, J.A. Kerr, M.J. Pilling, D. Stocker, J. Troe, W. Tsang, R.W. Walker, J. Warnatz, Evaluated kinetic data for combustion modelling: Supplement II. J. Phys. Chem. Ref. Data 34 (2005) 757.

[77] K. Narayanaswamy, P. Pepiot, H. Pitsch, A chemical mechanism for low to high temperature oxidation of n-dodecane as a component of transportation fuel surrogates, Combust. Flame 161 (2014) 866–884.

[78] S.J. Klippenstein, J.A. Miller, A.W. Jasper, Kinetics of propargyl radical dissociation, J. Phys. Chem. A 119 (2015) 7780−7791.

[79] C.F. Cullis, I.A. Read, Pyrolysis of vinylacetylene, Trans. Faraday Soc. 66 (1970) 920-929, doi:10.1039/TF9706600920.

[80] S.W. Benson, Radical processes in the pyrolysis of acetylene, Int. J. Chem. Kinet. 24, (1992) 217–237.

[81] J.P. Senosiain, J.A. Miller, The reaction of n- and i-C_4H_5 radicals with acetylene, J. Phys. Chem. A 111 (2007) 3740–3747.

[82] C. Doute, J.L. Delfau, R. Akrich, C. Vovelle, Chemical structure of atmospheric pressure premixed decane and kerosene flames, Combust. Sci. and Tech. 106 (1995) 327–344.